Journal of Polymer Science and Engineering 2024, 7(1), 4510.
https://doi.org/10.24294/jpse.v7i1.4510

Article

Low-cost ternary composite photocatalysts consisting of TiO_2, kaolinite and cement for an efficient organic waste decontamination in water

Kohobhange Karunadasa[1,*], Pannilage Madhushanka[2], Chinthan Manoratne[1]

[1] Materials Technology Section, Industrial Technology Institute, Colombo, 00700, Sri Lanka
[2] Postgraduate Institute of Science, University of Peradeniya, Peradeniya, 20400, Sri Lanka
*** Corresponding author:** Kohobhange Karunadasa, sujithkohobhange@yahoo.com

CITATION

Karunadasa K, Madhushanka P, Manoratne C. Low-cost ternary composite photocatalysts consisting of TiO_2, kaolinite and cement for an efficient organic waste decontamination in water. Journal of Polymer Science and Engineering. 2024; 7(1): 4510. https://doi.org/10.24294/jpse.v7i1.4510

ARTICLE INFO

Received: 1 February 2024
Accepted: 18 March 2024
Available online: 16 April 2024

Abstract: The present study demonstrates the fabrication of heterogeneous ternary composite photocatalysts consisting of TiO_2, kaolinite, and cement (TKCe), which is essential to overcome the practical barriers that are inherent to currently available photocatalysts. TKCe is prepared via a cost-effective method, which involves mechanical compression and thermal activation as major fabrication steps. The clay-cement ratio primarily determines TKCe mechanical strength and photocatalytic efficiency, where TKCe with the optimum clay-cement ratio, which is 1:1, results in a uniform matrix with fewer surface defects. The composites that have a clay-cement ratio below or above the optimum ratio account for comparatively low mechanical strength and photocatalytic activity due to inhomogeneous surfaces with more defects, including particle agglomeration and cracks. The TKCe mechanical strength comes mainly from clay-TiO_2 interactions and TiO_2-cement interactions. TiO_2-cement interactions result in $CaTiO_3$ formation, which significantly increases matrix interactions; however, the maximum composite performance is observed at the optimum titanate level; anything above or below this level deteriorates composite performance. Over 90% degradation rates are characteristic of all TKCe, which follow pseudo-first-order kinetics in methylene blue decontamination. The highest rate constant is observed with TKCe 1-1, which is 1.57 h^{-1} and is the highest among all the binary composite photocatalysts that were fabricated previously. The TKCe 1-1 accounts for the highest mechanical strength, which is 6.97 MPa, while the lowest is observed with TKCe 3-1, indicating that the clay-cement ratio has a direct relation to composite strength. TKCe is a potential photocatalyst that can be obtained in variable sizes and shapes, complying with real industrial wastewater treatment requirements.

Keywords: TiO_2; kaolinite; cement; composite photocatalyst; industrial wastewater treatment

1. Introduction

Rapid industrialization, agrochemical consumption, and limited disposal space have all contributed to the accumulation of organic waste in water bodies, which is responsible for significant environmental pollution [1]. Traditional wastewater treatment methods (alkaline hydrolysis) are less viable due to drawbacks such as high alkaline consumption, low treatment efficiency, and environmental pollution caused primarily by alkaline disposal [1]. The photo-catalyzed advanced oxidation method outperforms conventional treatment methods for organic waste decontamination in water. Photocatalytic degradation is a well-known advanced oxidation process due to its high efficiency and environmental friendliness when compared to other advanced oxidation processes, including the Photo-Fenton technique, which requires additional reagents [2]. TiO_2 is a well-known semiconductor photocatalyst that can decontaminate a wide range of organics and microorganisms while producing

inorganic species that are naturally harmless. This is mainly achieved via advanced oxidation, where organic waste decontamination is initiated by electron-hole pair generation under sunlight/UV irradiation, which is often used to mineralize a variety of organic pollutants in wastewater. Because of its high photocatalytic activity/stability, chemical/biological inertness, and low cost, TiO_2 has been widely used.

Photocatalysts can be utilized as a powder, membrane (immobilized on the surface of a suitable substrate), or composite material. TiO_2 powder is less effective as a photocatalyst alone because of its small specific surface area, low adsorption ability, photocatalyst agglomeration, and post-separation issues [1]. A supportive substrate that has a large surface area and a high adsorption capacity should be used to immobilize TiO_2 powder, which is an essential step to overcome these limitations. Photocatalyst immobilization can be accomplished on a variety of substrates. Powder/pellets, soft/thin, and rigid substrates are the three major classes that have often been used [3]. Activated carbon, clay, and volcanic ash are the best powder/pellet substrates for immobilizing photocatalysts. The soft/thin substrates fall within a broad range, including alumina, polyvinylidene difluoride, glass filters, cellulose fibers, and sponges [4–7]. TiO_2 can be immobilized on a substrate using one of two methods, including binders' incorporation or physically anchoring TiO_2 particles on a substrate [1]. Poor TiO_2 immobilization is caused by the use of organic/inorganic binders, including polyester resin, polyethylene, polypropylene, polyethylene glycol, and silicon adhesive [8–10]. Because the binders are typically organic in nature, they are highly susceptible to self-degradation (by TiO_2) when exposed to sunlight/UV light. TiO_2 particles, on the other hand, can submerge and agglomerate within the binder, resulting in decreased photocatalytic activity. The coating preparation is also imperfect and complex, resulting in a number of difficulties in controlling the uniformity and durability.

Apart from binder-based TiO_2 immobilization, clay is a better supportive substrate than many other types, making it a promising raw material for hybrid photocatalysts. TiO_2-clay photocatalysts differ in terms of both preparation and morphology [1]. The sol-gel process, which involves growing and anchoring nanosized TiO_2 particles on the clay surface, has been widely used to produce clay-based photocatalysts. Despite the basic characteristics of the sol-gel process, preparation methods involve a diverse set of techniques and raw materials, resulting in a highly diversified synthesis process. Titanium butoxide, $TiCl_4$, $TiOSO_4$, and titanium tetra-isopropoxide are common titanium precursors used in the sol-gel process [11–20]. The various techniques that are often used in sol-gel synthesis, including hetero-coagulation, hydrothermal treatment, calcination, ultrasonic agitation, supercritical drying, and intercalation, make the preparation significantly diverse [11–20]. The well-known clay types that are frequently used in TiO_2-based hybrid photocatalysts are kaolinite, hectorite, rectorite, palygorskite, montmorillonite, vermiculite, and allophane [11–16]. However, because these clay-based products are primarily in powder/particle/aggregate forms, commercial applications are limited due to constraints associated with the implementation of large-scale reactors [11–20]. High manufacturing costs, post-separation issues, short-term durability, and installation difficulties, particularly in large industrial treatment tanks, are major limitations of

existing TiO_2-clay-based photocatalysts [1]. The latter highlights the importance of hybrid photocatalysts that can be easily integrated with commercial wastewater treatment units.

Existing techniques are limited to laboratory scale or prototypes, and their commercial applications are imperfect. Due to the low stability/durability of the photocatalysts and engineering constraints that are related to reactor design, they fail to meet industrial waste disposal standards. From an industrial standpoint, low-cost, long-lasting photocatalysts that can be easily integrated into commercial wastewater treatment units are essential. Furthermore, having a readily available photocatalyst that can be easily synthesized on a large scale is more important. The authors of the present study recently developed a novel composite preparation method based on mechanical compression and heat treatment, resulting in a stable binder-free graphite and clay composite electrode [21–25]. Following a similar technique, authors recently developed efficient binary photocatalysts that are composed of raw materials, including TiO_2 and clay (kaolinite/MMT), resulting in improved photocatalytic activity and mechanical strength [26,27]. However, authors also found that ternary composites that are related to graphite-clay composite electrodes outperform the binary electrodes, revealing that such ternary composites result in matrix enhancements [23,24]. Based on a similar hypothesis, the current study demonstrated the fabrication of a ternary TiO_2-clay-cement composite photocatalyst (TKCe) for the first time. The TKCP offers numerous advantages, including high photocatalytic activity, mechanical stability, mouldability, chemical-free surface regeneration, and long shelf life, resulting in an effective photocatalyst that can bridge the gap between lab scale and commercial products.

2. Material and methods

2.1. Materials

Nippon Aerosil Co. Ltd., Japan, provided TiO_2 (Degussa P25 powder) with 56 nm particles. Sigma-Aldrich Ltd., USA, provided the raw minerals, including kaolinite (>99%, 1.2 μm particles) and methylene blue (>99%). The cement (>98%, average particle size 1.5 μm) was obtained from the Department of Geology at the University of Peradeniya in Sri Lanka.

2.2. TKCe block fabrication

To prepare composite suspensions, a fixed amount of TiO_2 (80%) was mixed in distilled water with various clay and cement (total 20%) ratios and then continuously stirred at 1000 rpm using an overhead agitator (IKA, Germany) for 3 h. TKCe 1-3, TKCe 1-1, and TKCe 3-1 were prepared in 25 g by combining kaolinite and cement in the following ratios: 1:3, 1:1, and 3:1. TKCe blocks with dimensions of 4 cm × 4 cm × 0.8 cm were fabricated by applying a 125,000 N vertical ram force for 30 min to a partially dried composite material that was uniformly packed inside a specially designed steel mould. TKCe blocks were then calcined for 2 h at 600 ℃ in a high-temperature furnace (Nebertherm), resulting in a TiO_2-kaolinite-cement heterogeneous photocatalyst (**Figure 1**). The TKCe photocatalytic activity was

determined using modified blocks with an untreated top surface. To accomplish this, the TKCe blocks' side and bottom surfaces were uniformly painted, except the top surface, which serves as the active exterior, facilitating photocatalytic disintegration.

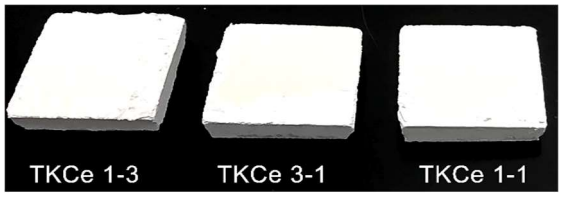

Figure 1. TKCe blocks prepared with different kaolinite and cement ratios.

2.3. TKCe block characterization

To characterize the TKCe blocks and raw materials, an X-ray diffractometer (Rigaku Ultima IV, Japan) equipped with a copper target X-ray generator ($\lambda_{CuK\alpha1}$-0.154056 nm), a secondary beam curved graphite monochromator, and a D/tex Ultra detector were used. An X-ray beam generated under standard tube conditions, including a 40 kV tube voltage and a current of 30 mA, was used to analyze the powdered samples. The samples were scanned between 15° and 80° at 2° min^{-1} to obtain diffractograms. The X-ray beam geometry was carefully optimized, with the divergence, scattering, and receiving slits all fine-tuned by 2/3°, 2/3°, and 0.45 mm, respectively. The Rietveld refinement on XRD profiles was performed using an advanced WPPF (whole powder pattern fitting) component that was integrated with the PDXL X-ray powder diffraction software. The refined diffractograms were analyzed with the PDXL integrated X-ray powder diffraction software, which was linked to the ICDD (International Centre for Diffraction Data) database. The composition analysis was achieved via the Relative Intensity Ratio (RIR) module that is available with powder diffraction software. The crystallite size estimation related to both anatase and rutile was carried out accurately by analyzing refined diffractograms using the Halder-Wagner model available with PDXL software.

The flexural strength was calculated by substituting the force at rupture of a TKCe strip that was measured using a universal testing machine (Testometric, UK). To accomplish this, the TKCe strip was carefully placed horizontally on the Testometric universal testing machine's supporting stage, and the force at the fracture point was measured upon collision with a load that was vertically lowered at a rate of 2 mm min^{-1}.

$$\sigma_f = (FL / 2bd^2) \quad (1)$$

where σ_f, F, L, b, and d stand for flexural strength, force at the fracture point, supporting span length (2.00 cm), TKCe strip width (1.3 cm), and TKCe strip depth (0.8 cm), respectively [28].

The TKCe series was examined using a scanning electron microscope (ZEISS EVO LS15, Germany), which produced well-resolved images at a constant accelerating voltage of 20 kV. The FT-IR spectra were collected in an attenuation total reflection module (ATR) with a diamond puck (sample compartment) using a Bruker Tensor 27 spectrometer (Germany). The samples were scanned between 600 and 4000 cm^{-1} at a resolution of 4 cm^{-1}, yielding a transmittance spectrum from which the vibration frequencies corresponding to IR bands were obtained. TGA/DSC analysis

(TA Instruments SDTQ600, USA) was used to determine the thermal profile and stability of kaolinite.

2.4. TKCe photocatalytic activity determination

Methylene blue degradation in the presence of TKCe was measured using a UV-visible spectrophotometer (UV-1800 Shimadzu, Japan, at λ_{max} = 664 nm). Each TKCe block was placed in a crystallization flask (150 mL), followed by 100 mL of methylene blue solution (1.56×10^{-5} mol dm^{-3}). The reaction vessels were exposed to sunlight for 2.5 h, with absorbance measurements taken every thirty minutes (**Figure 2**). The dye concentration (C_{MB}) after each consecutive irradiation was determined carefully using a calibration plot that was preliminarily constructed with known methylene blue concentrations. The calibration plot was constructed using the UVProbe software, which is interfaced with the UV-Vis spectrophotometer. The irradiated methylene blue concentration was determined directly from the previously installed calibration plot. The entire experiment was conducted in direct sunlight, with an average irradiation of 400 W m^{-2} (intensity). After determining the methylene blue concentration in relation to the control sample, the percentage degradation (D_R) and the pseudo-first-order rate constant (k) were calculated using the following relationships [29].

$$D_R = [(C_0 - C_{MB}) / C_0] \times 100\% \quad (2)$$

$$lnC_{MB} = -kt + lnC_0 \quad (3)$$

where C_0 (1.56×10^{-5} mol dm^{-3}), C_{MB}, and t denote the initial concentration of methylene blue, concentration at time t, and time, respectively.

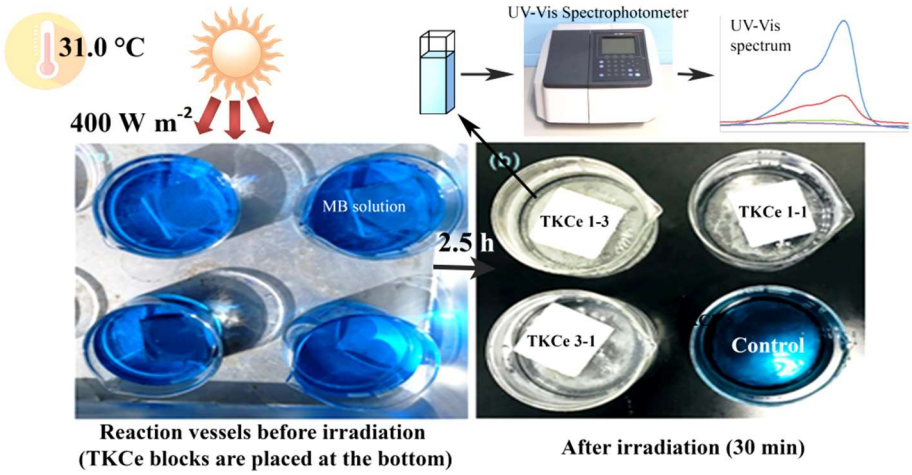

Figure 2. TKCe photocatalytic activity determination under natural sunlight.

3. Results and discussion

According to previous studies, the TiO_2 amount that can effectively be incorporated into a binary TiO_2-clay-based composite photocatalyst is found to be 60%, greater than which the composite stability is drastically reduced, causing multiple surface cracks [26]. In the present study, the TiO_2 percentage that can be incorporated into the composite photocatalysts is greater than the previously fabricated binary composite photocatalyst. This is mainly due to cement incorporation as an additional mineral phase, which results in high TiO_2 loading capacity without

deteriorating the composite mechanical strength. The clay itself can only increase the TiO_2 loading capacity up to some extent, but the clay-cement combination makes the composite architectural framework quite stronger, which results in stable ternary composite photocatalysts. The high TiO_2 loading capacity is an advantage that makes TiO_2 surface concentration very high, resulting in a high photocatalytic activity. This is a good indication for the advancement of solid-state composite engineering, which highlights the incorporation of minerals together, including clay and cement, that can significantly improve the photocatalysts' properties and performance.

The clay firing is a major step that led to a strong photocatalyst matrix, which mainly resulted from the dehydroxylation, integrating the clay mineral with other composite components. Among the many clay types available, kaolinite was chosen in the current study due to its low cost, high abundance, and platy sheet-like structure, which allow easy processing of the material at high compressibility [26]. **Figure 3** exhibits a TGA/DTA thermogram, which reveals that kaolinite typically undergoing dehydroxylation at 500 ℃, resulting in a rigid clay matrix. Therefore, the firing temperature was set at 600 ℃ to ensure complete dehydroxylation. It also reveals that spinal crystallization takes place at 1000 ℃, followed by mullite and crystobalite formation, which typically occurs above 1100 ℃.

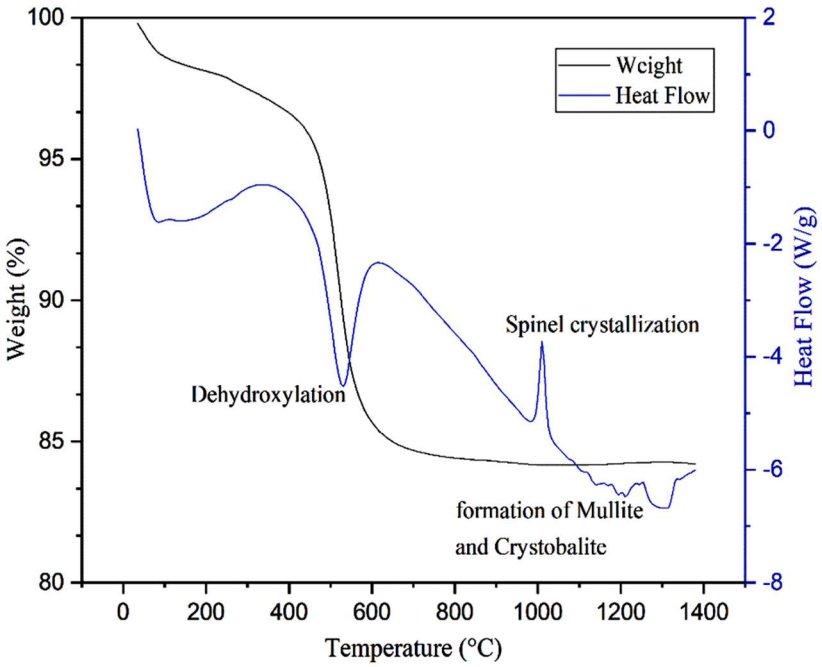

Figure 3. TGA-DSC curves related to kaolinite.

The TKCe photocatalytic activity and the mechanical strength are both important factors that determine the industrial-level feasibility. TKCe 1-1 accounts for the highest photocatalytic activity and mechanical strength, revealing that the 1:1 kaolinite to cement ratio resulted in an effective composite matrix (**Table 1**). Over 98% degradation rate (D_R) is observed with TKCe 1-1, which is the highest among all binary composite photocatalysts that are fabricated previously and raw TiO_2 [26,27]. The authors' previous study observed a very low D_R (72.5%) and pseudo-first-order rate constant (k = 0.28 h^{-1}) related to raw TiO_2 when used in powder form, which is

mainly due to the ultra-fine particle nature of TiO_2, which results in a colloidal suspension where the tiny particles are dispersed throughout the entire solution [26]. This is caused by poor sunlight penetration and scattering through the suspension, which results in ineffective sample irradiation [26]. TKCe 1-1 also accounts for the highest pseudo-first-order rate constant (k), which is higher than binary composites, and many photocatalysts test against methylene blue, including TiO_2 nanotrees (0.346 h^{-1}), TiO_2 nanobelts (0.026 h^{-1}), multilayer TiO_2 coating on HDPE (0.27–0.43 h^{-1}), and GO-ZnO-Cu nanocomposite (0.246 h^{-1}) [26,30–32] (see **Table 1** and **Figure 4**). The plots (C vs. time and 1/C vs. time) both account for a nonlinear relationship, which confirms the deviation from the zero and the second-order reaction kinetics (**Figure 4**). TKCe 1-3 and TKCe 3-1 both accounted for a higher %degradation and k compared to previously developed binary TiO_2-kaolinite (TKCP) and TiO_2-kaolinite-MMT composite (TKMCP) photocatalysts. These binary composites have shown a less than 95% degradation rate in comparison to TKCe, which exhibits a D_R > 98% (**Table 1**). TKCe 1–1 rate constant, which is 1.57 h^{-1}, is quite similar to that of TKMCP (1.55 h^{-1}) and is greater than that of TKCP (0.58 h^{-1}) [26,27].

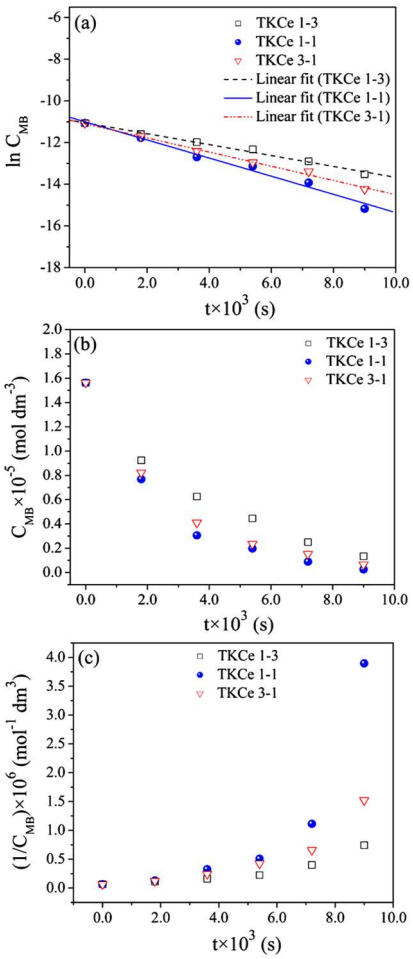

Figure 4. TKCe kinetic studies related to methylene blue degradation **(a)** ln C_{MB} vs. time (C_{MB}-Methylene blue concentration); **(b)** C_{MB} vs. time; **(c)** 1/C_{MB} vs. time.

Table 1. TKCe flexural strength, DR, and pseudo first-order rate constant.

Composite	D_R (%)	k (h^{-1})	σ_f (MPa)
TKCe 1-3	91.4	0.94	6.44
TKCe 1-1	98.4	1.57	6.97
TKCe 3-1	95.8	1.22	5.67

The mechanical strength of TKCe follows a similar trend as photocatalytic activity, with the highest observed with TKCe 1-1 (6.97 MPa), implying that the optimal cement percentage is critical for a better composite matrix (**Table 1**). The much lower or higher cement percentages result in comparatively deteriorated properties and performance of TKCe. In that sense, the highest D_R, σ_f, and k were observed in TKCe 1-1, which is considered the composite with the optimum kaolinite to cement ratio; the composites that deviate from the optimum ratio account for comparatively low D_R, σ_f, and k (see **Table 1**). Among the rest of the TKCe composites, the composite with more cement accounts for a stronger matrix than the one with the lowest cement fraction, which is TKCe 3-1. In contrast, the composite with a high clay fraction results in better photocatalytic activity than the one with a low clay fraction, which is TKCe 1-3 (**Table 1**). TKCe 1-1 mechanical strength is greater than that of binary composites, including TKCP (3.55 MPa) and TKMCP (5.83 MPa), that were fabricated previously [26,27]. Therefore, an optimum clay-cement combination simultaneously results in high photocatalytic activity and mechanical strength, which is observed in TKCe 1-1, revealing that proper raw material combinations can have a significant impact on composite properties.

The improved photocatalytic activity and mechanical strength related to TKCe 1-1 can be explained by considering four factors, including anatase to rutile ratio, crystallite size, calcium titanate percentage, and morphology. The anatase to rutile ratio in each composite is determined using an X-ray diffraction analysis, and the results are given in **Table 2**. The authors of the current article revealed that the same TiO_2 powder underwent a measurable phase transition at low temperatures, resulting in a composition change of approximately 25% at 650 °C [33]. Such phase transitions are prevented in binary composites that are fabricated using clay. This is because clay eventually acts as a phase transformation barrier and predominantly undergoes dehydroxylation, preventing anatase from rutile transformation [26,27]. In the present study, kaolinite also acts as a barrier for anatase to rutile conversion, preventing the phase transformation, which results in a marginal change in rutile percentage (**Table 2**). Kaolinite not only serves as a phase transition barrier but also provides an architectural framework for strengthening the composite matrix.

Table 2. TKCe composition and crystallite size (anatase and rutile).

Composite	Composition (%)				D_{cryst} (nm)	
	Anatase	Rutile	$CaTiO_3$	$CaCO_3$	Anatase	Rutile
TKCe 3-1	81.6	14.5	2.9	1.1	16.7	21.1
TKCe 1-1	78.9	14.6	4.5	2.0	17.0	24.0
TKCe 1-3	68.2	13.8	12.2	5.8	11.3	22.1

D_{cryst} - Crystallite size.

TKCe composites are negative for characteristic kaolinite XRD peaks, indicating that dehydroxylation occurred completely, resulting in metakaolinite, which is amorphous in nature (please see **Figures 5** and **6**). The FT-IR spectra related to TKCe provide clear evidence for the amorphization of kaolinite, which is confirmed by the absence of characteristic kaolinite IR bands between 1250–600 cm^{-1} (in-plane Si-O stretching vibration at 1114 and 1007 cm^{-1}, OH vibration of inner and outer Al-OH bonds at 912 cm^{-1}, Si-O-Al stretching vibration at 788 and 748 cm^{-1}) and emergence of an amorphous SiO_2 peak at 1070 cm^{-1} (**Figure 7**). This anti-symmetric Si-O stretching band is unique to metakaolinite, and the absence of bands in composites at 3689 and 3619 cm^{-1}, which correspond to the stretching vibration of hydroxyl, ensures complete dehydroxylation [34].

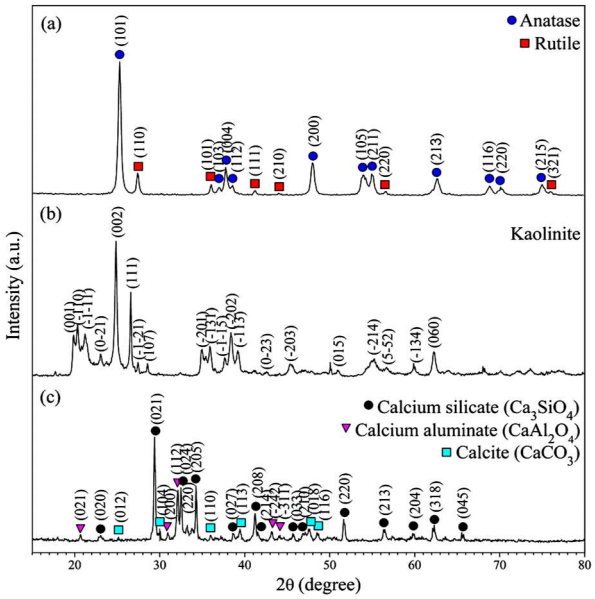

Figure 5. X-ray diffractograms of raw materials at room temperature **(a)** TiO_2; **(b)** kaolinite; **(c)** cement.

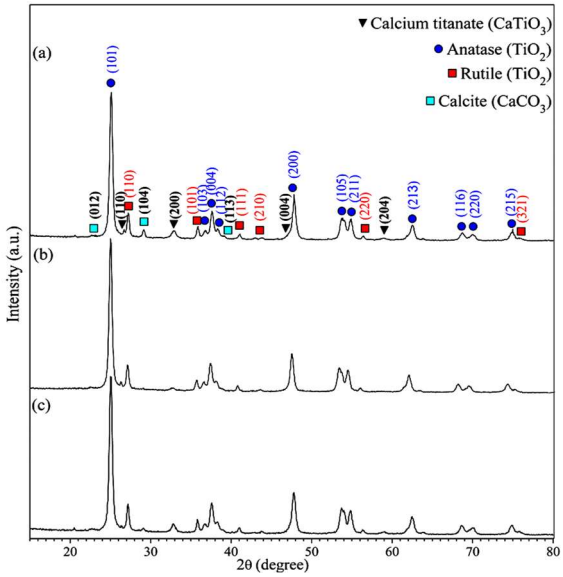

Figure 6. X-ray diffractograms of TKCe **(a)** TKCe 1-3; **(b)** TKCe 3-1; **(c)** TKCe 1-1.

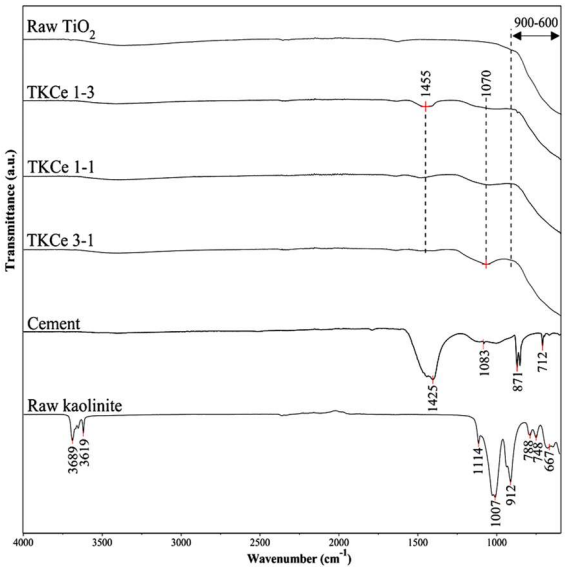

Figure 7. FT-IR spectra of raw materials and composites.

However, the situation is somewhat different when incorporating cement as a ternary phase that consumes anatase to produce calcium titanate ($CaTiO_3$) instead of undergoing phase transformation, resulting in a considerable reduction in anatase percentage (**Table 2**). This is clearly reflected by the anatase and rutile percentages that are observed in composites and raw TiO_2, exhibiting a significant reduction in anatase percentage unlike rutile, which is quite similar in magnitude (**Table 2**). The calcium titanate formation typically occurs at high temperatures, which are above 900 °C [35]. In the present study, $CaTiO_3$ emerged at 600 °C, revealing that such formation is likely induced by a highly compressed matrix, which is responsible for low-temperature titanate formation. This is a good indication of mechanical activation that mainly results from the highly compressed matrix, which triggers the thermal conversion of minerals within the composite even at low to moderate temperatures. $CaTiO_3$ formation begins with the thermal decomposition of calcite, which results in CaO (calcite from cement, see **Figure 5**). However, calcite decomposition is a high-temperature process that typically occurs above 700 °C [36].

In the present study, mechanical compression is implemented as a fabrication technique that leads to a highly compressed material matrix, which eventually experiences very high matrix stress. The composite heating also accounts for the further increase in matrix stress where the composite matrix tries to regain stability via either thermal decomposition or matrix distortion. The thermal decomposition is more effective than the matrix deformation, where matrix stability is likely achieved via material loss, resulting in a low matrix stress [36,37]. This explains why calcite is decomposed even at temperatures that are well below the typical decomposition temperature. The CO_2 removal during calcite decomposition is likely to reduce the matrix stress by increasing the internal space, which is mainly caused by material loss [36]. Therefore, unlike non-compressed materials, materials that are under high compression strain can easily undergo thermal conversions even at low to moderate temperatures.

The reaction between CaO and TiO_2 produced orthorhombic $CaTiO_3$, which is the stable phase below 1200 ℃; this is more pronounced in TKCe, which contains more cement (**Figure 6** and **Table 2**). During $CaTiO_3$ formation, the reaction is most likely propagated in the following sequence [35,36].

$$At\ 600\ ℃(2\ h)$$

$$CaCO_{3(s)} \xrightarrow{\Delta} CaO_{(s)} + CO_{2(g)}$$

$$CaO_{(s)} + TiO_{2(s)}(\text{anatase}) \xrightarrow{\Delta} CaTiO_{3(s)}$$

The TKCe X-ray diffractograms provide clear evidence for titanate formation and the amorphization of certain cement phases that are available at room temperature. The absence of characteristic cement phases in TKCe, including calcium silicate and aluminates, is a better indication for cement amorphization, which is also reflected in TKCe FT-IR spectra (**Figure 7**). Raw cement exhibits the characteristic vibrational modes at 871, 1083, and 1425 cm^{-1}, which are corresponded to CO_3^{2-} stretching (out-of-plane), Si-O-Si stretching, and CO_3^{2-} stretching (asymmetric) modes, respectively (**Figure 7**) [38]. These modes are mainly caused by primary constituents in cement, including $CaCO_3$ and calcium silicate (**Figure 6**). A low, intense, broad titanate FT-IR vibration band can be seen in all composites (1455 cm^{-1}), but it is more pronounced in TKCe 1-3, which has the highest titanate percentage (**Figure 7**) [39]. The most distinctive cement IR bands, which correspond to calcite CO_3^{2-} vibrations, and $CaTiO_3$ fingerprint bands are masked by a broad Ti-O-Ti stretching vibration band that typically appears between 900 and 600 cm^{-1} (see **Figure 7**) [26,27].

In TiO_2-clay binary composites that are recently developed, the dehydroxylation typically results in Ti-O-Si and Al-O-Ti bond formation that ensures a strong composite matrix [26,27]. However, in the present study, $CaTiO_3$ is directly involved in the material architectural framework, increasing the mechanical strength in addition to the Ti-O-Si and Al-O-Ti formations that are reflected by TKCe's very high flexural strength (**Tables 1** and **2**). However, $CaTiO_3$ in excess can negatively affect the matrix uniformity, which results in the lowest flexural strength and photocatalytic activity that are clearly noticeable in TKCe 1-3 (**Tables 1** and **2**). This indicates that an optimum $CaTiO_3$ level is important to have a uniform composite matrix with improved properties. Numerous studies have revealed that anatase itself is a relatively poor photocatalyst, but anatase and rutile mixtures are better photocatalysts with a wide range of applications [40]. The optimum titanate level also accounts for the proper anatase to rutile ratio, which is quite essential to obtaining an efficient photocatalyst with high activity, which is clearly reflected in TKCe 1-1 (**Table 1**).

Anatase crystallite size and photocatalytic activity have a direct relationshp that is well noticeable in TKCe 1-3, which has the smallest anatase crystallites, resulting in the lowest catalytic activity. The more cement in TKCe can produce excess $CaTiO_3$, during the production of which anatase crystallites are greatly consumed upon the reaction with CaO that likely damages the crystallites, resulting in small anatase crystallites. A small anatase crystallite size is a strong indication of the matrix defects that are typically generated during titanate formation. The titanate formation via anatase incorporation is confirmed by a significant decrease in anatase size and a marginal change in rutile crystallite size, indicating that rutile is less important in titanate formation, most likely due to structural disparity and low abundance (see

Table 2). However, up to a certain level, the titanate formation is positively affected by TKCe properties and performance, resulting in improved mechanical strength and catalytic activity. This is in better agreement with the high DR observed with TKCe 1-1, which has the largest anatase crystallites (**Table 2**). However, this is somewhat opposite when the titanate percentage increases above the optimum level, where the excess $CaTiO_3$ is likely to damage the composite matrix, destabilizing the anatase lattice, which results in small crystallites.

The TKCe composition-matrix correlations are clearly reflected in SEM micrographs, which reveal the structural alterations that occurred under mechanical and heat treatment. The SEM images reveal that a uniform composite surface is more pronounced in TKCe 1-1 compared to both TKCe 1-3 and TKCe 3-1, which have somewhat less uniform surfaces. In contrast to binary TiO_2-clay composite photocatalysts, cement incorporation induces raw material amalgamation, resulting in small spherical composite particles that are packed together, resulting in a compressed composite matrix (**Figure 8**).

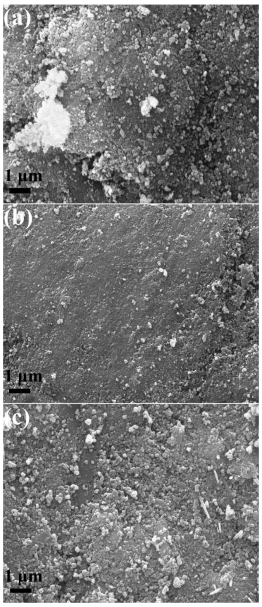

Figure 8. SEM images exhibiting TKCe surface **(a)** TKCe 3-1; **(b)** TKCe 1-1; and **(c)** TKCe 1-3. The particle agglomeration and surface defects are more pronounced in both TKCe 1-3 and TKCe 3-1 compared to TKCe 1-1. TKCe 1-1 exhibits a uniform matrix with fewer surface defects, facilitating a highly compressed surface for effective photocatalytic activity.

The nature of the composite particles, including shape and size, is important in determining the composite's compressibility under hydraulic pressing. However, it is obvious that the size of such composite particles is determined by their composition, particularly the ratio of kaolinite to cement.

The TKCe 1-1 SEM micrograph clearly exhibits fewer surface defects and a well-organized, uniform composite matrix, which explains the improved mechanical strength and photocatalytic activity of TKCe 1-1. In contrast to TKCe 1-1, both TKCe 1-3 and TKCe 3-1 have partially compressed matrixes with more surface defects, including particle agglomerates and cracks. This explains why mechanical

compression and heat treatment are more effective when the optimal matrix composition is used, resulting in a uniform matrix with low surface defects. It is important to have composite particles that can undergo effective mechanical compression (high compressibility), resulting in a highly compressed matrix. In contrast, both TKCe 1-3 and TKCe 3-1 resulted in poor compressibility, leaving more surface defects, including particle agglomerates and cracks. Therefore, the deviation from optimum raw material ratios accounted for a less uniform composite matrix with comparatively higher surface defects, which are mostly particle agglomerations, forming as a result of low compressibility. The latter accounts for partially compressed composite particles that are still noticeable in both TKCe 1-3 and TKCe 3-1 SEM micrographs.

The TiO_2 immobilization technique described here is very useful for large-scale commercial photocatalyst fabrication, with a focus on high-capacity wastewater treatment plants that are powered by renewable sunlight or UV irradiation. The simple chemical-free fabrication process makes commercial-level TKCe production more feasible, requiring minimal supervision and machinery and yielding a high output. TKCe has several advantages, including easy fabrication, low cost, free of hazardous chemicals, high production capacity with minimal machinery/supervision, non-self-degradability, easy disposal, easy installation in pilot-scale reactors, compatibility with both batch and flow reactors, and environmental and user-friendliness.

4. Conclusions

An industrially feasible TiO_2-kaolinite-cement composite photocatalyst is prepared using inexpensive raw materials via a straightforward method. The fabrication route is intended to avoid additional reagents, making the process more economical, faster, and environmentally friendly (green technology). The TKCe can be manufactured in a variety of shapes and sizes to match the reactor dimensions, reducing engineering constraints when upgrading the lab-scale product to pilot-scale reactors. The physical properties of TKCe are primarily determined by the clay-cement ratio, where the optimum ratio, which is 1:1, exhibits the highest photocatalytic activity and flexural strength. This is mainly due to a uniform TKCe matrix with fewer surface defects, which resulted from its high compressibility. Composites with clay-cement ratios below or above the optimum ratio exhibit lower mechanical strength and photocatalytic activity due to an inhomogeneous surface with more defects, such as particle agglomeration and cracks. TKCe mechanical strength is primarily derived from clay-TiO_2 interactions and TiO_2-cement interactions. TiO_2-cement combination results in $CaTiO_3$, which significantly improves matrix interactions; however, the best composite performance is achieved at the optimal titanate level; anything above or below this level negatively affects composite performance. The TiO_2 immobilization technique that is described here is very useful for large-scale commercial photocatalyst fabrication, with a focus on high-capacity wastewater treatment plants powered by renewable sunlight or UV irradiation. The simple chemical-free fabrication process enables commercial-scale TKCe production with minimal supervision and machinery, resulting in a high production capacity.

Author contributions: Conceptualization, KK; methodology, KK and PM; software, KK and PM; validation, KK; formal analysis, KK and PM; investigation, KK; resources, KK; data curation, KK and PM; writing—original draft preparation, KK; writing—review and editing, KK; visualization, KK; supervision, KK; project administration, CM; funding acquisition, CM. All authors have read and agreed to the published version of the manuscript.

Funding: The financial support for this research is provided by the National Research Council of Sri Lanka under grant number 20–014.

Conflict of interest: The authors declare no conflict of interest.

References

1. Szczepanik B. Photocatalytic degradation of organic contaminants over clay-TiO_2 nanocomposites: A review. Applied Clay Science. 2017; 141: 227-239. doi: 10.1016/j.clay.2017.02.029
2. Lofrano G, Rizzo L, Grassi M, et al. Advanced oxidation of catechol: A comparison among photocatalysis, Fenton and photo-Fenton processes. Desalination. 2009; 249(2): 878-883. doi: 10.1016/j.desal.2009.02.068
3. Lazar M, Varghese S, Nair S. Photocatalytic Water Treatment by Titanium Dioxide: Recent Updates. Catalysts. 2012; 2(4): 572-601. doi: 10.3390/catal2040572
4. Djafer L, Ayral A, Ouagued A. Robust synthesis and performance of a titania-based ultrafiltration membrane with photocatalytic properties. Separation and Purification Technology. 2010; 75(2): 198-203. doi: 10.1016/j.seppur.2010.08.001
5. Damodar RA, You SJ, Chou HH. Study the self cleaning, antibacterial and photocatalytic properties of TiO_2 entrapped PVDF membranes. Journal of Hazardous Materials. 2009; 172(2-3): 1321-1328. doi: 10.1016/j.jhazmat.2009.07.139
6. Liu L, Liu Z, Bai H, et al. Concurrent filtration and solar photocatalytic disinfection/degradation using high-performance Ag/TiO_2 nanofiber membrane. Water Research. 2012; 46(4): 1101-1112. doi: 10.1016/j.watres.2011.12.009
7. Bedford NM, Pelaez M, Han C, et al. Photocatalytic cellulosic electrospun fibers for the degradation of potent cyanobacteria toxin microcystin-LR. Journal of Materials Chemistry. 2012; 22(25): 12666. doi: 10.1039/c2jm31597a
8. Tennakone K, Tilakaratne CTK, Kottegoda IRM. Photocatalytic degradation of organic contaminants in water with TiO_2 supported on polythene films. Journal of Photochemistry and Photobiology A: Chemistry. 1995; 87(2): 177-179. doi: 10.1016/1010-6030(94)03980-9
9. Tennakone K, Kottegoda IRM. Photocatalytic mineralization of paraquat dissolved in water by TiO_2 supported on polythene and polypropylene films. Journal of Photochemistry and Photobiology A: Chemistry. 1996; 93(1): 79-81. doi: 10.1016/1010-6030(95)04141-9
10. Kumara GRRA, Sultanbawa FM, Perera VPS, et al. Continuous flow photochemical reactor for solar decontamination of water using immobilized TiO_2. Solar Energy Materials and Solar Cells. 1999; 58(2): 167-171. doi: 10.1016/S0927-0248(98)00200-1
11. Kibanova D, Trejo M, Destaillats H, et al. Synthesis of hectorite–TiO_2 and kaolinite–TiO_2 nanocomposites with photocatalytic activity for the degradation of model air pollutants. Applied Clay Science. 2009; 42(3-4): 563-568. doi: 10.1016/j.clay.2008.03.009
12. Papoulis D, Komarneni S, Panagiotaras D, et al. Halloysite–TiO_2 nanocomposites: Synthesis, characterization and photocatalytic activity. Applied Catalysis B: Environmental. 2013; 132-133: 416-422. doi: 10.1016/j.apcatb.2012.12.012
13. Zhao D, Zhou J, Liu N. Characterization of the structure and catalytic activity of copper modified palygorskite/TiO_2 (Cu^{2+}-PG/TiO_2) catalysts. Materials Science and Engineering: A. 2006; 431(1-2): 256-262. doi: 10.1016/j.msea.2006.06.001
14. Kameshima Y, Tamura Y, Nakajima A, et al. Preparation and properties of TiO_2/montmorillonite composites. Applied Clay Science. 2009; 45(1-2): 20-23. doi: 10.1016/j.clay.2009.03.005
15. Machado LCR, Torchia CB, Lago RM. Floating photocatalysts based on TiO_2 supported on high surface area exfoliated vermiculite for water decontamination. Catalysis Communications. 2006; 7(8): 538-541. doi: 10.1016/j.catcom.2005.10.020
16. Nishikiori H, Shindoh J, Takahashi N, et al. Adsorption of benzene derivatives on allophane. Applied Clay Science. 2009; 43(2): 160-163. doi: 10.1016/j.clay.2008.07.024

17. Chong MN, Lei S, Jin B, et al. Optimisation of an annular photoreactor process for degradation of Congo Red using a newly synthesized titania impregnated kaolinite nano-photocatalyst. Separation and Purification Technology. 2009; 67(3): 355-363. doi: 10.1016/j.seppur.2009.04.001
18. Mamulová Kutláková K, Tokarský J, Kovář P, et al. Preparation and characterization of photoactive composite kaolinite/TiO_2. Journal of Hazardous Materials. 2011; 188(1-3): 212-220. doi: 10.1016/j.jhazmat.2011.01.106
19. Zhang GK, Ding XM, He FS, et al. Low-Temperature Synthesis and Photocatalytic Activity of TiO_2 Pillared Montmorillonite. Langmuir. 2008; 24(3): 1026-1030. doi: 10.1021/la702649v
20. Ding Z, Hu X, Yue PL, et al. Synthesis of anatase TiO_2 supported on porous solids by chemical vapor deposition. Catalysis Today. 2001; 68(1): 173-182. doi: 10.1016/S0920-5861(01)00298-X
21. Karunadasa KSP, Manoratne CH, Pitawala HMTGA, et al. A potential working electrode based on graphite and montmorillonite for electrochemical applications in both aqueous and molten salt electrolytes. Electrochemistry Communications. 2019; 108: 106562. doi: 10.1016/j.elecom.2019.106562
22. Karunadasa KSP, Rathnayake D, Manoratne C, et al. A binder-free composite of graphite and kaolinite as a stable working electrode for general electrochemical applications. Electrochemical Science Advances. 2021; 1(4). doi: 10.1002/elsa.202100003
23. Rathnayake DT, Karunadasa KSP, Wijekoon ASK, et al. Low-cost ternary composite of graphite, kaolinite and cement as a potential working electrode for general electrochemical applications. Chemical Papers. 2022; 76(10): 6653-6658. doi: 10.1007/s11696-022-02314-w
24. Madhushanka PMH, Karunadasa KSP, Gamini Rajapakse RM, et al. Low-cost composite electrode consisting of graphite, colloidal graphite and montmorillonite with enhanced electrochemical performance for general electroanalytical techniques and device fabrication. Chemical Papers. 2023; 78(1): 633-643. doi: 10.1007/s11696-023-03086-7
25. Rathnayake DT, Karunadasa KSP, Wijekoon ASK, et al. Polyaniline-conjugated graphite–montmorillonite composite electrode prepared by in situ electropolymerization for supercapacitor applications. Chemical Papers. 2023; 77(5): 2923-2928. doi: 10.1007/s11696-022-02646-7
26. Karunadasa KSP, Wijekoon ASK, Manoratne CH. TiO_2-kaolinite composite photocatalyst for industrial organic waste decontamination. Next Materials. 2024; 3: 100065. doi: 10.1016/j.nxmate.2023.100065
27. Gunarathne PPB, Karunadasa KSP. Low-cost heterogeneous composite photocatalyst consisting of TiO_2, kaolinite and MMT with improved mechanical strength and photocatalytic activity for industrial wastewater treatment. Insight - Mechanics. 2023; 6(1). doi: 10.18282/m.v6i1.597
28. Temenoff JS. Biomaterials: The Intersection of Biology and Materials science, 1st ed. Pearson prentice Hall; 2008. pp. 151-159.
29. Alkaykh S, Mbarek A, Ali-Shattle EE. Photocatalytic degradation of methylene blue dye in aqueous solution by $MnTiO_3$ nanoparticles under sunlight irradiation. Heliyon. 2020; 6(4): e03663. doi: 10.1016/j.heliyon.2020.e03663
30. Kasanen J, Salstela J, Suvanto M, et al. Photocatalytic degradation of methylene blue in water solution by multilayer TiO_2 coating on HDPE. Applied Surface Science. 2011; 258(5): 1738-1743. doi: 10.1016/j.apsusc.2011.10.028
31. Al-Rawashdeh NAF, Allabadi O, Aljarrah MT. Photocatalytic Activity of Graphene Oxide/Zinc Oxide Nanocomposites with Embedded Metal Nanoparticles for the Degradation of Organic Dyes. ACS Omega. 2020; 5(43): 28046-28055. doi: 10.1021/acsomega.0c03608
32. Dharma HNC, Jaafar J, Widiastuti N, et al. A Review of Titanium Dioxide (TiO_2)-Based Photocatalyst for Oilfield-Produced Water Treatment. Membranes. 2022; 12(3): 345. doi: 10.3390/membranes12030345
33. Karunadasa KSP, Manoratne CH. Microstructural view of anatase to rutile phase transformation examined by in-situ high-temperature X-ray powder diffraction. Journal of Solid State Chemistry. 2022; 314: 123377. doi: 10.1016/j.jssc.2022.123377
34. Sengyang P, Rangsriwatananon K, Chaisena A. Preparation of zeolite N from metakaolinite by hydrothermal method. Journal of Ceramic Processing Research. 2015; 16(1): 111-116.
35. Křenek T, Kovářík T, Pola J, et al. Nano and micro-forms of calcium titanate: Synthesis, properties and application. Open Ceramics. 2021; 8: 100177. doi: 10.1016/j.oceram.2021.100177
36. Karunadasa KSP, Manoratne CH, Pitawala HMTGA, et al. Thermal decomposition of calcium carbonate (calcite polymorph) as examined by in-situ high-temperature X-ray powder diffraction. Journal of Physics and Chemistry of Solids. 2019; 134: 21-28. doi: 10.1016/j.jpcs.2019.05.023

37. Karunadasa KSP. Dehydration of Calcium Chloride as Examined by High-temperature X-ray Powder Diffraction. International Multidisciplinary Research Journal. 2019; 4: 37-43.
38. Cho J, Waetzig GR, Udayakantha M, et al. Incorporation of Hydroxyethylcellulose-Functionalized Halloysite as a Means of Decreasing the Thermal Conductivity of Oilwell Cement. Scientific Reports. 2018; 8(1). doi: 10.1038/s41598-018-34283-0
39. Portia SAU, Srinivasan R, Elaiyappillai E, et al. Facile synthesis of Eu-doped $CaTiO_3$ and their enhanced supercapacitive performance. Ionics. 2020; 26(7): 3543-3554. doi: 10.1007/s11581-020-03494-9
40. Ohtani B, Prieto-Mahaney OO, Li D, et al. What is Degussa (Evonik) P25? Crystalline composition analysis, reconstruction from isolated pure particles and photocatalytic activity test. Journal of Photochemistry and Photobiology A: Chemistry. 2010; 216(2-3): 179-182. doi: 10.1016/j.jphotochem.2010.07.024